Received: 25 June 2019 | Revised: 13 January 2020 | Accepted: 13 January 2020

DOI: 10.1002/er.5227

RESEARCH ARTICLE

INTERNATIONAL JOURNAL OF ENERGY RESEARCH WILEY

Ag-doped PbS thin films by nebulizer spray pyrolysis for solar cells

S. Rex Rosario[1] | I. Kulandaisamy[1] | K. Deva Arun Kumar[2] | K. Ramesh[2] | Hala A. Ibrahium[3,4] | Nasser S. Awwad[5]

[1]PG & Research Department of Physics, Arul Anandar College, Karumathur, India

[2]Department of Physics, Indian Institute of Science, Bengaluru, India

[3]Department of Biology, Faculty of Science, King Khalid University, Abha, Saudi Arabia

[4]Department of Biology, Nuclear Materials Authority, P.O. Box 530, El Maadi, Egypt

[5]Research Centre for Advanced Materials Science (RCAMS), King Khalid University, P.O. Box 9004, Abha 61413, Saudi Arabia

Correspondence
S. Rex Rosario, PG & Research Department of Physics, Arul Anandar College, Karumathur, India.
Email: kingrosario@gmail.com

Funding information
Department of Science and Technology, India, Grant/Award Number: DST-FIST/C-297/2015; King Khalid University, Grant/Award Number: RCAMS/KKU/006-19

Summary

Silver (Ag)-doped PbS (PbS:Ag) thin films of 616 to 745 nm in thickness were prepared on glass substrates via cost-effective nebulizer spray method by adding different Ag levels from 2% to 8% at 200°C. For solar cell applications, the effect of Ag doping concentration on structural, morphological, optical, photoluminescence, and electrical chattels of PbS thin film has been studied. X-ray diffraction pattern confirmed the polycrystalline behavior of the prepared PbS:Ag films with cubic crystalline nature. The crystalline size and texture coefficient were increased by increasing Ag doping concentration. From the morphological studies by scanning electron microscope (SEM) and atomic force microscope (AFM), the grain size of the films and surface roughness values were increased for the increase in Ag doping concentration. EDS spectra confirmed the existence of Ag, Pb, and S elements in the select 6% Ag-doped PbS film. Peaks related to silver oxide started to emerge at 6% of Ag doping level. The optical direct band gap value was reduced from 1.51 to 1.17 eV for Ag doping from 2% to 6% and thereby slightly increased as 1.79 eV for 8% Ag doping level. For all PbS:Ag films, the photoluminescence spectrum emitted a strong near band edge (NBE) emission at approximately 580 nm, meaning better optical quality. Hall effect measurements evidenced that Ag doping provides enhancement on the characteristics of mobility, carrier concentration, and resistivity with p-type conducting nature. The observed high carrier concentration and low resistivity values were 4.32×10^{14} cm^{-3} and 80 Ωcm, for 6% Ag-doped PbS film. The FTO/CdS/PbS:Ag heterostructure solar cell was formed from 6% Ag-doped film.

KEYWORDS

hall effect, PbS:Ag, solar cell, thin film, XRD

1 | INTRODUCTION

The thin film deposition of novel material with different methods is the main aim in the development of photovoltaic research. Selenium (Se), tellurium (Te), gallium (Ga), and indium (In) based photovoltaic devices exhibit various levels of efficiency from 17.5% to 28.8%.[1] But the main problem with these materials is their high cost and scarcity, which, will in, turn fail to meet the energy demands of the society.[2] It is, therefore, essential to search for earth's abundant elements such as lead sulfide (PbS) for using it as absorbing layer in solar cell. PbS, a semiconductor material with a narrow band gap (0.4 eV), varies from other semiconductors with regard to temperature and the

possibility of altering its band gap. Also, it is sensitive towards its grain size, which allows it to become a promising candidate for preparing nanostructured devices.[3] PbS is a p-type semiconductor with face-centered cubic (fcc) crystal structure that belongs to the IV-VI semiconductor.[4,5] Also, it has a large exciton Bohr radius as 18 nm for 0.1-m effective mass and 7 nm for 0.25-m effective mass of both electron and hole. Lead sulfide (PbS) is worthy of preparing the absorber layer for heterojunction solar cells owing to its enhanced optical and electrical properties.[6,7] PbS with its large exciton Bohr radius helps in quantum confinement effect and allows it to adjust the optical band gap through the formation of nanostructure PbS material as well as with the fact of p-type conductivity it possesses so that its high optical absorption coefficient makes it expedient for photovoltaic applications.[8] PbS with its wide range of application is proposed to be used in gas sensors,[9] field-effect transistors,[10] infrared detectors,[11] solar radiation control coatings,[12] solar selective absorber coating,[13] Pb^{2+} ion-selective sensors,[14] pesticidal electrochemical biosensors,[15] and increasing solar cell efficiency.[16]

Saikia et al developed a structure as Glass/SnO_2/CdS/PbS/HgTe and obtained the conversion efficiency of about 1.668%.[17] Moreno-Garcia et al[18] chemically prepared CdS/Bi_2S_3/PbS, Bi_2S_3/PbS, and ZnS/Bi_2S_3/PbS heterostructure using PbS absorber layer and CdS/ZnS buffer with conversion efficiency from approximately 0.01% to 0.4%. CdS/PbS solar cell device was fabricated by Sattarian et al[19] with solar cell efficiency of about approximately 1.31% through the chemical bath method.

However, doping with host PbS with different metal ions foster to enhance and control its optical and electrical properties. Many reports are available for doping on PbS with various elements as Sn, Al, Sb, Cu, Sr, and Cd.[20-25] The present study focuses on doping of silver (Ag) ions on PbS to attain device quality film, crack-free surface with tunable microstructure and with suitable optoelectronic and transport properties. Many deposition techniques have been carried out to prepare PbS thin films like electrodeposition, SILAR, CBD, and spray pyrolysis. Here, PbS:Ag thin films were prepared through nebulizer spray pyrolysis (NSP). The main advantages of the NSP techniques are as follows: (a) low cost (b) user-friendly, (c) air pressure, and (d) the substrate to nozzle distance and substrate temperature are adjustable. This is the first work with Ag doping concentration on the structural, morphological, optical, and photovoltaic properties of NSP-prepared PbS films, according to the literature survey. The present work aims to improve Ag's doping concentration in order to manufacture solar cells. The systematic analysis was done on the outcome of Ag doping concentration on the properties of prepared lead sulfide films.

2 | EXPERIMENT AND CHARACTERIZATION

Analytical grade lead nitrate ($PbNO_3$), thiourea (CS $[NH_2]_2$), and silver nitrate ($AgNO_3$) were used as starting materials for lead, sulfur, and silver, respectively, to prepare a thin film of PbS:Ag compound on amorphous glass substrates. The substrates were well cleaned with chromic acid, distilled water, methanol, and acetone for the deposition process. In order to prepare the precursor solution, the spray solution with 1:1M ratio of lead nitrate and thiourea was dissolved in 10 mL of deionized water. Then the spray solution was kept in magnetic stirrer for the complete dissolution after adding the different concentrations (2, 4, 6, and 8 wt%) of Ag dopant, respectively. The hot plate arrangement was used to attain 200°C on the surface of the substrate. The air compressor was used to allow pressured air into the spray solution to convert the liquid solution into fine droplets to dissociate and condense as PbS on the substrate with an area of 2.5 cm × 2.5 cm having thickness of 1.33 mm maintained at 200°C. With the adjustable screw arrangement, the distance between the deposition surface and the spray nozzle was set at 5 cm. Same NSP technique was preferred to prepare CdS layer by taking 0.1M of cadmium chloride and thiourea, respectively, in 10 mL of distilled water at 310°C.

For analyzing the structure, surface morphology, elemental composition, and optical and electrical properties, the prepared PbS:Ag thin films were characterized. PbS:Ag films thickness were determined using model number SJ-301stylus profilometer. The analysis on structural properties was made via X-ray diffractometer (PAN analytical X' Pert PRO) with CuK_α radiation. By using scanning electron microscope (SEM) (EVO 18 ZEISS) and EDS, the morphology and elemental composition of the films were analyzed. Absorption/transmittance spectra and optical band gap measurements were done with the help of Lambda Perkin Elmer UV-Vis Spectrophotometer in the range of 200 to 1200 nm. *I-V* measurements were performed by utilizing Keithley source-meter model number 2450.

3 | RESULTS AND DISCUSSIONS

3.1 | Structural studies

Figure 1A visualizes the X-ray diffraction (XRD) pattern of the prepared PbS:Ag with different Ag doping concentrations from 2% to 8% mixed in the precursor solution at 200°C using NSP. The preferred orientations were along (111), (200), (220), (311), (222), and (400) planes for the

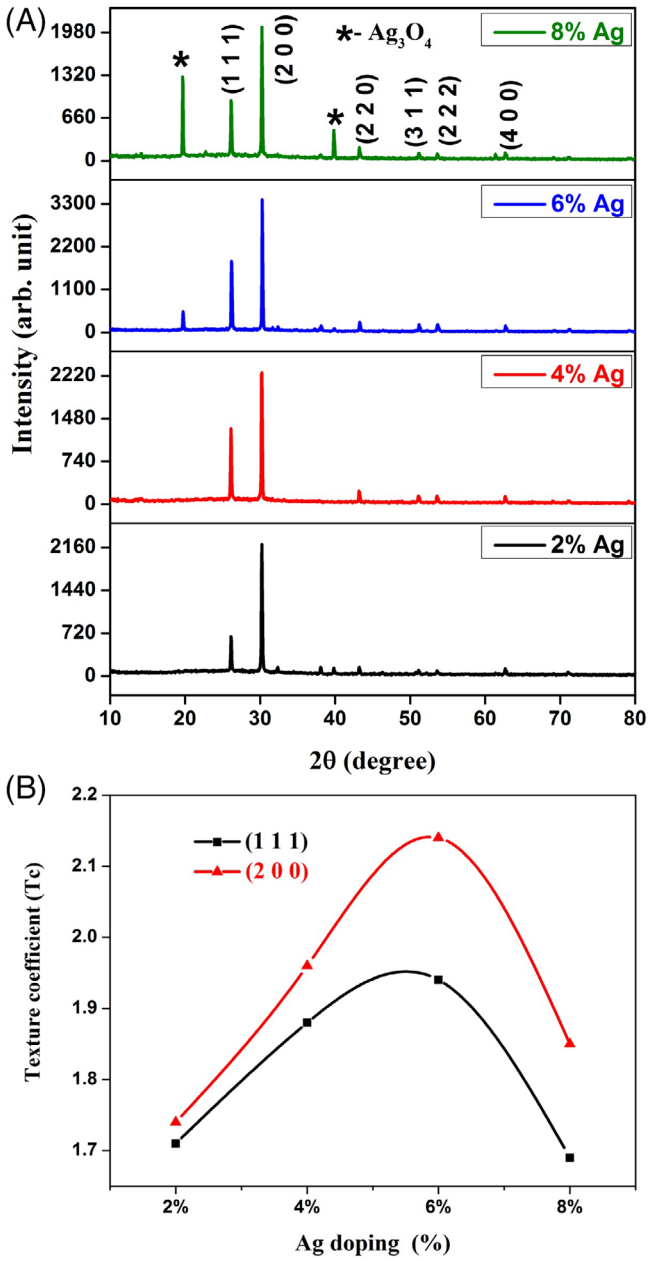

FIGURE 1 A, X-ray diffraction (XRD) patterns of Ag-doped PbS thin films with different doping levels. B, Texture coefficient variation with respect to different Ag doping levels [Colour figure can be viewed at wileyonlinelibrary.com]

prepared PbS:Ag thin films. These diffraction peaks fit with the standard JCPDS data file reference code well: 77-0244,[23] and also, it assigned as cubic crystal with polycrystalline nature. The whole XRD spectrum exposes a strong peak along (200) plane, indicating that the plane has minimal surface energy for the high orientation of the crystallites relative to others. Puiso et al[26] and Gadave et al[27] also projected same kind of high intense peak along (200) plane. The existed peaks in the XRD pattern manifest the increase in intensity on increasing Ag doping concentration up to 6%. At the same time, peaks related to Ag started to emerge at 6% of Ag doping level. The obtained intensity of Ag-doped film is slightly increased up to 6% Ag, which signifies that the Ag^{+} ions are incorporated into the regular lattice site of Pb^{2+} ions. The same nature of the increase in intensity was also observed by Touati et al.[28] Further, the decrease in intensity was perceived for the increase of Ag doping at 8%. This peak reduction may possibly occurs by the slight variation in the Ag (1.26 Å) ionic radius with Pb (1.20 Å), which leads to some lattice distortion or crystal imperfections because the Ag^{+} ions can disturb the crystalline improvement of host Pb^{2+}. Additionally, the PbS (200) peak's full width at half maximum (FWHM) increased, and the peak position was marginally moved to the lower angle side, which denote the reduction in crystallite size for 8% Ag. The same kind of peak reduction of host PbS film was already reported by Ravisankar et al[29] for Gd-doped PbS thin films with a higher ionic radius. Two supplementary peaks associated with Ag_3O_4 at $2\theta = 19.65°$ along (020) plane and 39.76° along (121) plane were observed for 6% and 8% Ag-doped films as a consequence of lattice disorder. The obtained additional Ag_3O_4 peaks related to JCPDS file no. 84-1261 mentioned as (*) in the XRD pattern. From the proper structural analysis, we conclude that the 8% Ag strongly affects the purity of pure PbS phase; nevertheless, by creating an impurity phase ie, Ag_3O_4, and indicates the formation of mixed phase due to the dissimilar ionic radius of Pb and Ag.

The crystallite size (D) of the deposited PbS:Ag films was determined by the Debye-Scherrer relationship using line broadening value.[30]

$$D = \frac{0.9\lambda}{\beta\cos\theta}. \quad (1)$$

Here, D, λ, β, and θ indicate crystallite size, wavelength, line broadening, and the Bragg angle, respectively. The crystallite size enhanced from 44 to 53 nm with increasing Ag dopant level up to 6%, since Pb ions were remarkably substituted by Ag ions. Further, it reduced to 44 nm at 8% Ag doping level as a result of interstitial occupation of excess of Ag ions, which causes change in the Pb^{2+} lattice arrangement. The crystallite size augmentation indicates the enrichment in crystalline quality, and so reduction in grain boundary occurs for PbS:Ag thin films; this also further diminishes the grain boundary scattering.[31]

The defects of the PbS:Ag films were quantified by calculating the microstrain (ε) and dislocation density (δ) using Williamson and tangent relations.[32,33]

$$\varepsilon = \frac{\beta\cot\theta}{4}, \quad (2)$$

TABLE 1 Thickness and structural properties of Ag-doped PbS thin films

Ag doping Concentration, %	Thickness, nm	(hkl)	Crystallite Size, nm	Dislocation Density (lines.m^{-2})	Strain	Lattice constant (Å) a = 5.934 Å
2	685	111	42	0.5655	0.00365	5.916
		200	44	0.5184	0.00303	
4	710	111	43	0.5312	0.00354	5.928
		200	47	0.4490	0.00282	
6	745	111	46	0.4729	0.00333	5.932
		200	53	0.3611	0.00252	
8	616	111	44	0.5227	0.00351	5.920
		200	44	0.5073	0.00301	

$$\delta = \frac{1}{D^2}, \tag{3}$$

where θ is the Bragg angle and D is the size of crystallites; the variation of ε and δ values of Ag-doped PbS films are presented in Table 1. To identify the particular material as good semiconducting material, the microstrain/dislocation density values should be low. The calculated ε and δ values were low for 6% PbS:Ag film, which shows that the film has lesser crystalline defect than the others and the obtained values are 0.00252 and 0.36×10^{15} nm^{-2}, respectively.

The crystal orientation of the PbS:Ag films were identified through the calculation of texture coefficient (TC) by below formula.[23]

$$\mathrm{TC(hkl)} = \frac{I(\mathrm{hkl})/I_0(\mathrm{hkl})}{N_r^{-1}\sum I(\mathrm{hkl})/I_0(\mathrm{hkl})}, \tag{4}$$

where I(hkl) and I_0(hkl) are perceived and established intensities and N is total reflections. If the TC(hkl) = 1, it indicates the growth occurrence in random manner, and when it is >1, the film growth occurs in a certain preferred orientation. In this study, the calculated TC value of PbS:Ag thin films were given in Figure 1B. In our case, TC is higher than 1 (TC(hkl) > 1) for all the Pb:Ag films. The calculated TC value for 6% Ag film is 2.19, which are same as our previous report.[34] This result suggests that lot of crystallites were gathered along (200) plane, and consequently, it may help to improve the electrical property.

PbS:Ag films' lattice constants (a) is calculated by the following relationship.[34]

$$\frac{1}{d^2} = \left\{\frac{h^2 + k^2 + l^2}{a^2}\right\}, \tag{5}$$

where d is the line spacing and (hkl) are the Miller indices. The calculated lattice constant values (a) from the above relationship for PbS:Ag films were nearer to JCPDS file no. 77-0244. With the rise in Ag doping level to 6%, the lattice constant values were significantly increased, and then it was further decreased. These variations may be due to the inclusion of the silver, and it causes local changes in host PbS lattice. The lattice constant was decreased for 8% Ag-doped PbS film, which is attributed to the presence of new impurity phase (Ag_3O_4) owing to more Ag ions enter into specific lattice sites. In addition to it, some other reasons also suggested for the minimum lattice constant are as follows: The host lattice could be controlled by stain level,[35] the lattice mismatch between the ionic radius of substitute ions and host site radius.[36] Moreover, the nature of Ag_3O_4 structure is different (monoclinic) from host PbS structure, so that it could disturb the arrangement of crystal and consequently reduce the lattice constant value.

3.2 | Morphological studies

The morphological study of the metal sulfide thin films was analyzed by means of SEM instrument. Figure 2A-D illustrates the images from SEM for PbS:Ag films with different Ag doping concentrations from 2% to 8%. In SEM images, it is observed that the Ag ions are incorporated in PbS lattice; it established some important modifications as compared with the pure PbS film surface.[23] In general, the morphology of prepared nanostructure has considerable influence on the electrical properties. The SEM micrographs indicate the change of grain shape and size with various Ag doping concentration; 2% Ag-doped PbS film surface showed that the spherical shaped grains were randomly arranged on the surface with some cracks (Figure 2A). The morphological shape was slightly changed from small spherical to agglomerated spherical shaped grains with an increase of 4% Ag (Figure 2B). For the film coated with 6% Ag doping level, the surface looks

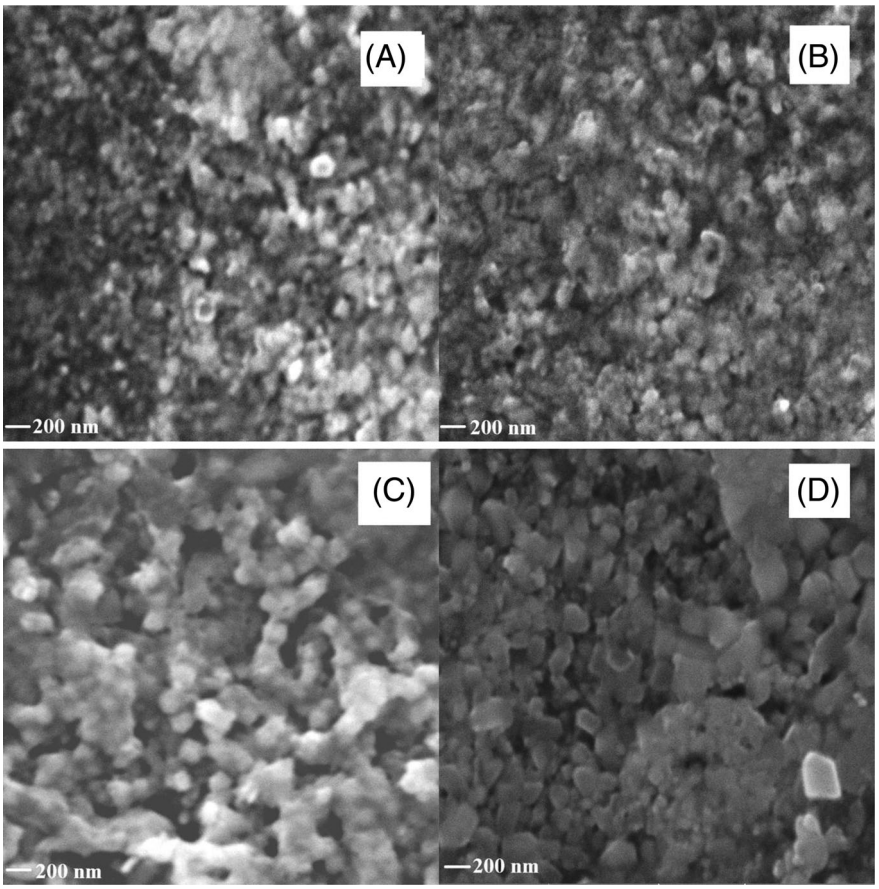

FIGURE 2 Scanning electron microscope (SEM) images of Ag-doped PbS thin films: (A) 2%, (B) 4%, (C) 6%, and (D) 8%

to be tightly packed with equal-sized spherical grains without any empty spaces (Figure 2C), which is similar to the previous report.[37] This kind of morphological structure can improve the electrical properties, which are well agreed with our electrical result (see Section 3.5). Finally, the Ag doping concentration rises to 8% (Figure 2D); the surface appears to be good, because of the presence of more silver element on PbS as evidenced from XRD. This may be attributed to the perfect replacement of Pb by Ag ions.

Surface topographical image was visualized via atomic force microscope (AFM) for the deposited thin films. By using the AFM, we can study the surface roughness of the deposited films. All films were scanned on an area of 2.5 μm × 2.5 μm to get morphological features on the surface. Figure 3A-D represents the 3D AFM images of PbS:Ag films for different Ag doping levels. Figure 3A shows the AFM image of 2% Ag-doped PbS film, which has spherical shaped uniform grains on the entire film surface. Figure 3B exhibits the improvement in grain size and roughness value for 4% Ag-doped PbS film. Further, the spherical grains are considerably increased by 6% PbS:Ag as given in Figure 3C. The surface roughness considerably increased as 34, 48, and 62 nm for 2%, 4%, and 6%, respectively; this is attributed to the increase of films' thickness. For a higher doping concentration of 8% PbS:Ag, the surface roughness value was reduced to 46 nm. This kind of roughness variation is well matched with the variation in crystallite size, evidence as of XRD study. Gassoumi et al presented similar change in surface roughness behavior for Mg^{2+}-doped PbS.[38] In Figure 3D, there is much reduction in grains as the higher level Ag doping fully occupied the growth behavior of host PbS.

Figure 4 illustrates the energy dispersive X-ray analysis (EDS) of 6% Ag-doped PbS film. From the depicted figure, the expected elements such as lead, sulfur, and silver were observed in the prepared film. The observed weight percentages are 45.26%, 50.12%, and 4.62% with corresponding to Pb, S, and Ag elements, respectively. It shows the incorporation of Ag ions into PbS structure. This incorporation factor can help with the influence of structural, optical, and electrical properties. The extra peak Si in the EDS spectrum other than Pb, S, and Ag peaks may come from the glass substrate.

3.3 | Optical studies

Usually, the optical absorption/transmittance performs a superior role for solar cell devices. The observed optical transmittance spectra of PbS:Ag films for different Ag doping percentage is given in Figure 5A. From the figure,

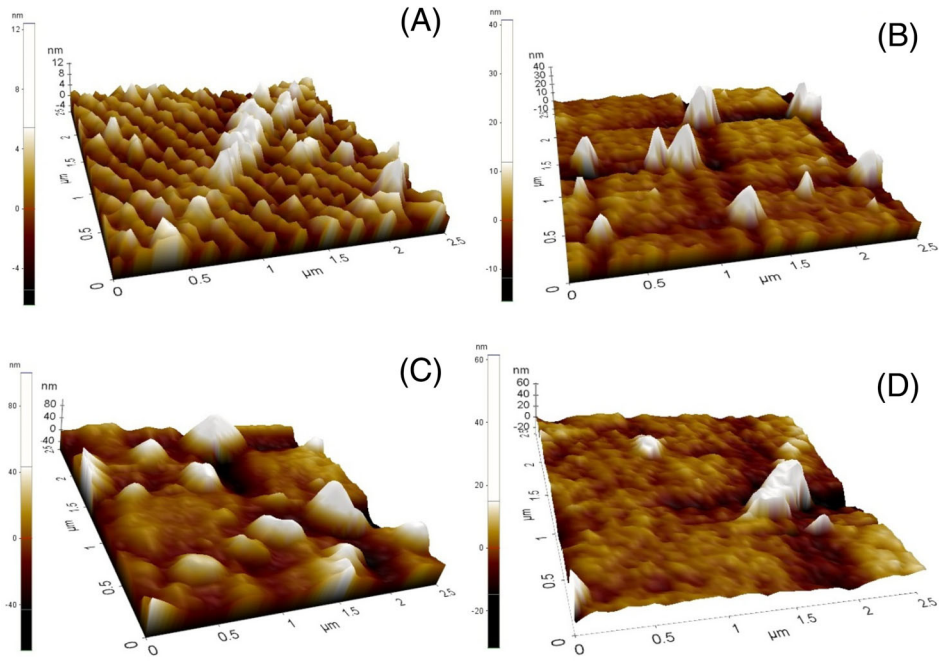

FIGURE 3 Atomic force microscope (AFM) images of Ag-doped PbS thin films: (A) 2%, (B) 4%, (C) 6%, and (D) 8% [Colour figure can be viewed at wileyonlinelibrary.com]

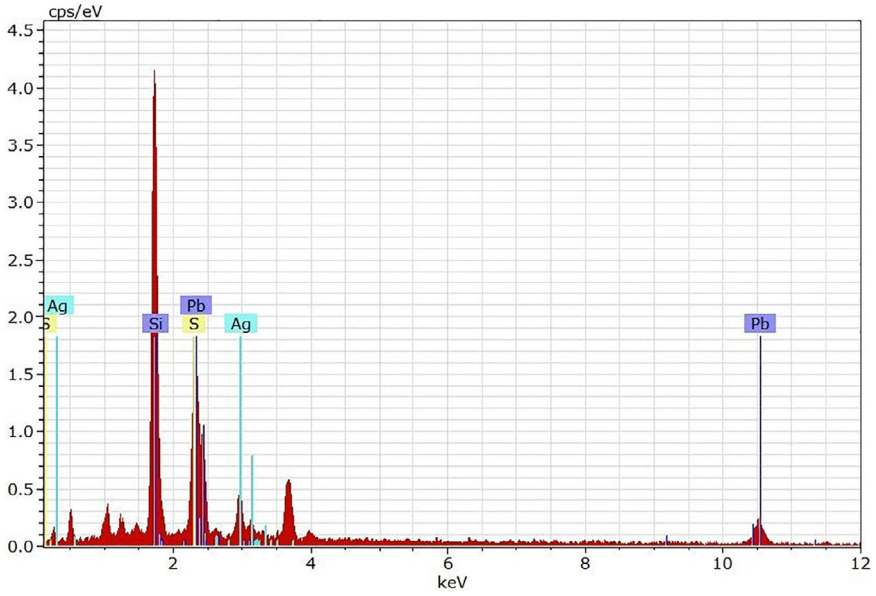

FIGURE 4 EDS spectrum of 6% Ag-doped PbS thin film [Colour figure can be viewed at wileyonlinelibrary.com]

the observed transmittance level was low up to the visible range (700 nm), and then it considerably increased along higher wavelength. The transmittance values are initially decreased up to 6% of Ag doping concentration, and then it was suddenly increased for 8%. The reasons are as follows: films thickness variation, increase in surface roughness, and light scattering of the film,[39] which is evidenced by the AFM study. The film thickness variation for various Ag doping percentage is listed in Table 1. The measured film thickness was increased up to 6% Ag and then decreased. This may be due to the peeling of the film on a further raise in the concentration of Ag (8%), which leads to thickness reduction. From transmittance spectra, the band edge at 680 nm (1.80 eV) was observed, this edge was initially moved to higher wavelength and then maintained to lower wavelength side for various doping levels. The transmittance linked to the exciting of the charge carrier from the valence band to the conduction band permits the change in the distance of optical band gap.[40] Bharathi and Sankar[41] also observed same type of variation on Mg doping concentration in chemical bath deposited PbS films. The prepared film's ability to absorb light is calculated by its coefficient of absorption. Using the Beer-Lambert Law equation as shown below,[42] the absorption coefficient (α) is determined as a function of wavelength (λ).

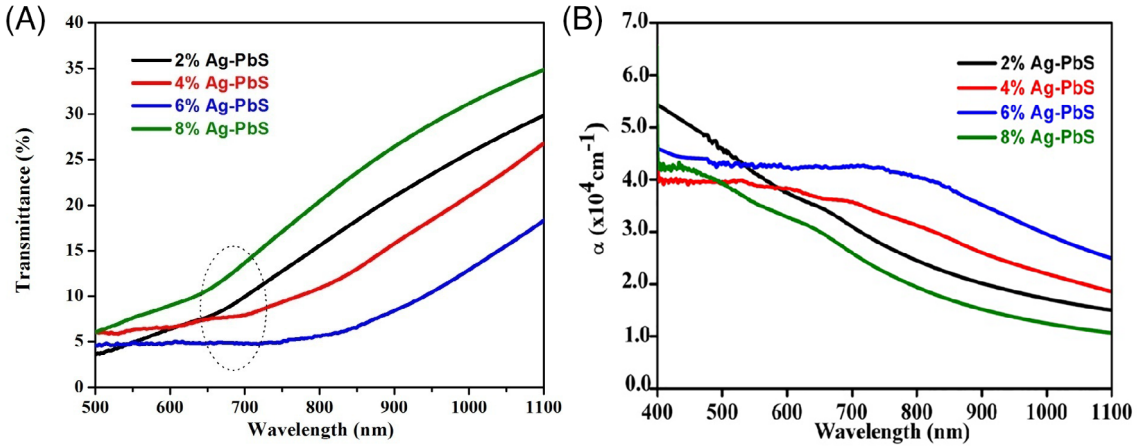

FIGURE 5 A, Transmittance spectra of PbS:Ag thin films with different doping levels. B, Absorption coefficient of PbS:Ag thin films with different doping levels [Colour figure can be viewed at wileyonlinelibrary.com]

$$\alpha = \ln\left(\frac{1}{\mathrm{T}}\right)/\mathrm{t}, \tag{6}$$

where the prepared films thickness and transmittance are mentioned as "t" and "T," respectively. Figure 5B shows the variation of α with λ for different Ag-doped PbS films. For all the prepared thin films, maximum absorption coefficient was observed in the visible region, indicates that it can perform as a absorber layer in solar cell device. It is shown that the α increased initially and then decreased exponentially on increase in the doping content. From the correlation,[42] PbS:Ag films band gap (E_g) was estimated as a function of absorption coefficient (α) vs incident photon energy ($h\nu$).

$$\alpha h\nu = B\left(\mathrm{h}\nu\text{-}E_g\right)^{\mathrm{n}}. \tag{7}$$

Here, $h\nu$, B, α, and E_g represent the usual meanings. In general, the optical properties may depend on film thickness, surface roughness, and crystallite size. Using Equation (7), the calculated band gap values are 1.51, 1.27, 1.17, and 1.79 eV for the different Ag doping concentrations 2%, 4%, 6%, and 8%, respectively, as shown in Figure 6A. Initially, measured band gap values were reduced and then increased with increasing the concentration of Ag doping, which may be due to an increase in film thickness as well as crystalline size.[34] Figure 6B illustrates the energy gap variations between valance band to conduction band with respect to different silver doping contents. As in the figure, it is clearly identified that the energy gap is low for 6% PbS:Ag, which absorbs more visible light than the other prepared films. Preetha et al[43] have presented

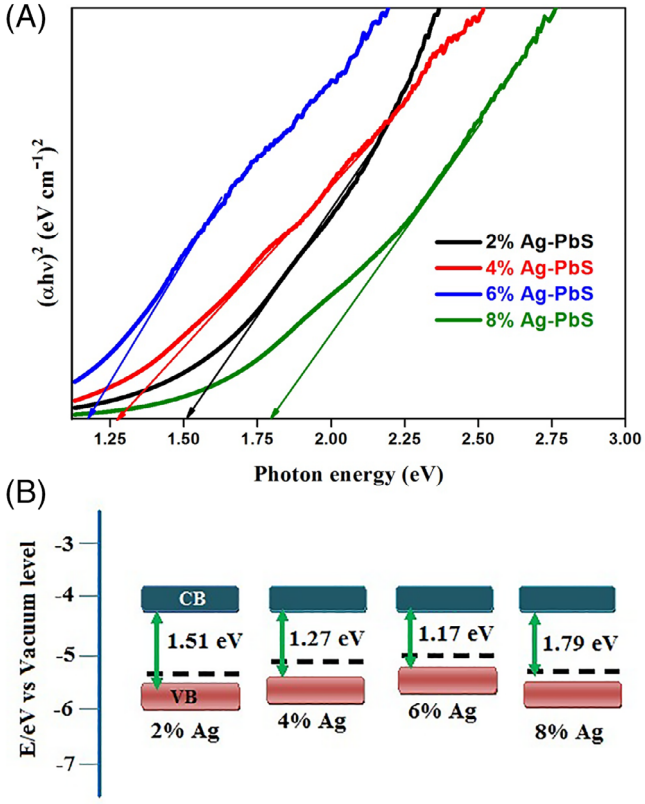

FIGURE 6 A, Band gap spectra of PbS:Ag thin films with different doping levels. B, Schematic diagram of band gap variation as a function of Ag doping level [Colour figure can be viewed at wileyonlinelibrary.com]

the similar band gap variations for aluminum (Al)-doped PbS films using chemical bath deposition method.

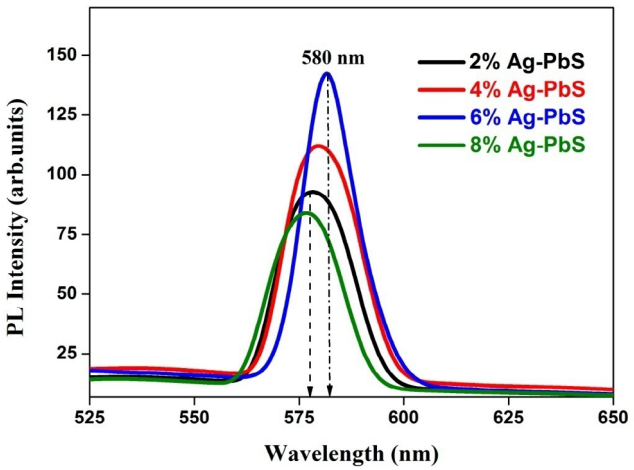

FIGURE 7 Photoluminescence spectra of PbS:Ag thin films with different doping levels [Colour figure can be viewed at wileyonlinelibrary.com]

3.4 | Photoluminescence spectra

Photoluminescence (PL) examination helps to measure the optical quality and defects present in the semiconducting material. At room temperature, the PL spectrum was measured with the 380-nm excitation wavelength. The PL spectrum of PbS:Ag thin films deposited with different Ag doping concentrations 2%, 4%, 6%, and 8% are presented in Figure 7. The emission peak should be in the range of 520 to 600 nm, which conforms to the PbS structure.[44] PL spectra were composed of one strong visible emission band positioned at about 580 nm in all the prepared PbS:Ag films. The strong peak observed at 580 nm corresponds to green emission. Recently, Cao et al[45] and Tohidi et al[46] observed the emission peaks at around 440 nm using the excited wavelength 330 nm for PbS thin films. They addressed that the observed PL emission at approximately 440 nm signifies the electrons transition from the conduction band edge to holes, present in interstitial Pb^{2+} sites. Also, they suggested that the emissions arose from the PbS nanostructures and not concerned with impurities like glass. Because this could be related to the surface trapped states in the PbS nanostructure. The intensity of the PL emission peak was increased considerably from 2% to 6% Ag-doped PbS films. This enhancement may represent the increasing population of Ag element on the host PbS lattice and decrease of space between Ag^{+} ions and Pb^{2+} ions. Whereas for higher doping level of 8% PbS:Ag film, the intensity was decreased, may be owing to increasing interstitial placement level of Ag ions near Pb sites, it leads to falling of the optical quality. Figure 7 indicates a small redshift for the Ag 6% film; consequently, there is a decrease in energy gap as evidenced from Figure 6A.

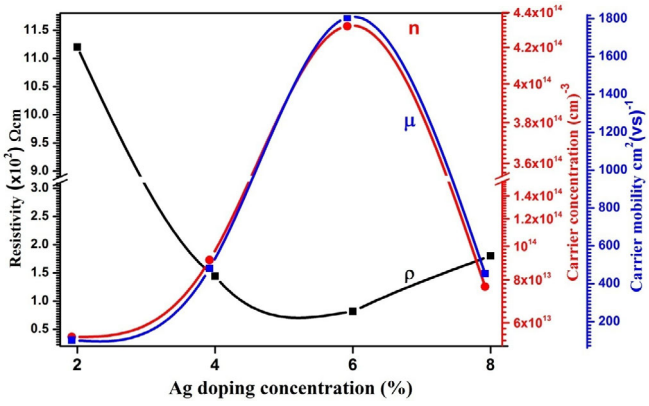

FIGURE 8 Electrical resistivity, carrier concentration, and mobility with respect to Ag-doped PbS thin films [Colour figure can be viewed at wileyonlinelibrary.com]

3.5 | Electrical studies

Electrical properties play a significant role in the solar cell device to increase conversion efficiency. The electrical parameters such as resistivity (ρ), carrier concentration (n), and mobility (μ) of all films were measured by hall effect measurement as given in Figure 8, and the values are presented in Table 2. Usually during doping, atoms can settle in interstitial or substitutional positions in the crystal lattice. As far as Ag atom is concerned, it can act either as p-type or n-type dopant in bulk semiconductors. Ag atom acts as p-type dopant when it is substituted for the cation, then as n-type dopant when it occupies the interstitial site. Here, large number of Ag^{+} ions replaces Pb^{2+} ions as substitution, up to 6% of Ag doping in the PbS lattice. So it provides extra hole because Ag acts as an acceptor; in turn, it increases the carrier concentration. Further, large numbers of Ag atoms occupy the interstitial sites in PbS lattice at 8% Ag doping. Therefore, Ag can act as a donor, resulting in a decrease of carrier concentration and an increase in resistivity of the film.[47] The observed high carrier concentration and mobility values are 4.32×10^{14} cm^{-3} and 1806 cm^2/vs, respectively, for 6% Ag-doped PbS film. The electrical study suggests that 6% Ag doping level plays a superior role in solar cell device fabrication.

3.6 | Solar cell studies on CdS/ PbS:Ag heterostructure

PbS-dependent solar cell was constructed with 6% of Ag doping, and their current and voltage (I-V) characteristics were studied. I-V characteristics of FTO/CdS/PbS:Ag in the dark and under illumination are shown in Figure 9. Good rectification property was observed for the prepared structure under dark and illumination conditions

TABLE 2 Electrical Properties of PbS:Ag films deposited with different doping concentrations

Ag doping Concentration, %	Roughness, nm	Resistivity, Ωcm	Carrier Concentration, cm^{-3}	Mobility, cm^2/vs	Type of Conductivity
2	34	1120	5.46×10^{13}	102	P
4	48	142	9.12×10^{13}	482	P
6	62	80	4.32×10^{14}	1806	P
8	46	180	7.64×10^{13}	453	P

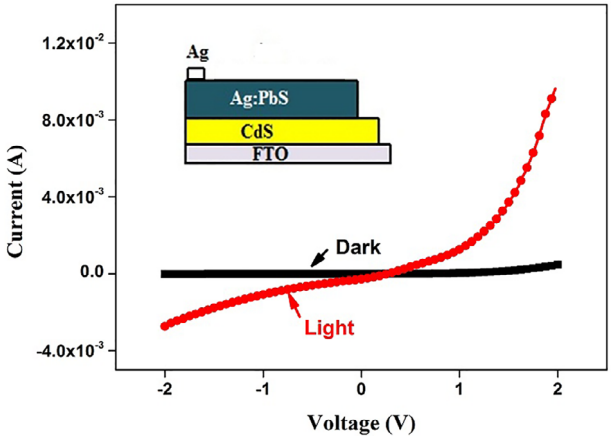

FIGURE 9 I-V characteristics of FTO/CdS/PbS:Ag heterostructure [Colour figure can be viewed at wileyonlinelibrary.com]

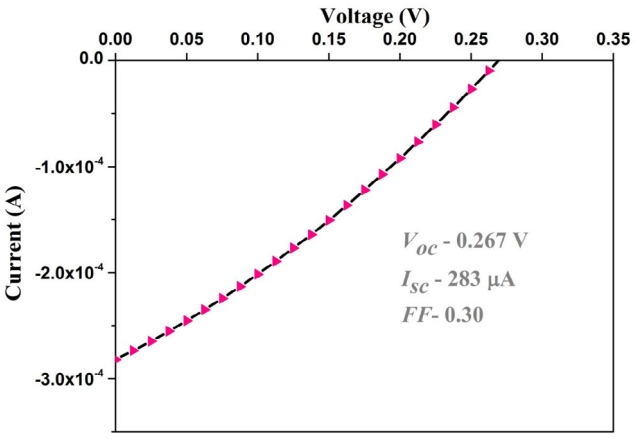

FIGURE 10 Illuminated I-V characteristics of FTO/CdS/PbS:Ag heterostructure [Colour figure can be viewed at wileyonlinelibrary.com]

through I-V characteristic. The inset of Figure 9 shows the formed heterostructure schematic diagram. An active area of 0.5 cm^2 was taken to study the I-V measurements under the illumination of 100 mW/cm^2. The illuminated I-V curve for FTO/n-CdS/p-PbS:Ag heterostructure is depicted in Figure 10. Using the examined relations,[48] the efficiency (η) and fill factor (FF) was also evaluated. When the prepared heterostructured solar cell was illuminated with a light of 100 mW/cm^2 in intensity, we observed the values of short circuit current density of approximately $0.285 \times 10^{-3} A/cm^2$, FF of approximately 0.30, open circuit voltage of approximately 0.263 V, and conversion efficiency of approximately 0.89% for 6% PbS:Ag. The reasons for the low efficiency are (a) some of the defects may be created during the preparation of p-type and n-type layer and (b) lattice mismatch between n-CdS and p-PbS layers, so that it may reduce the minority carrier's lifetime.[49] Based on the Anderson model, the FTO/CdS/PbS:Ag heterojunction energy band diagram was drawn and is given in Figure 11. The figure exhibits as the valance bands separation is high when compared with the conduction band edges which links p-PbS:Ag and n-CdS layers. Therefore, this device can capably separate the electron-hole pairs automatically; it generates large number of photo carriers. The energy gap of PbS:Ag

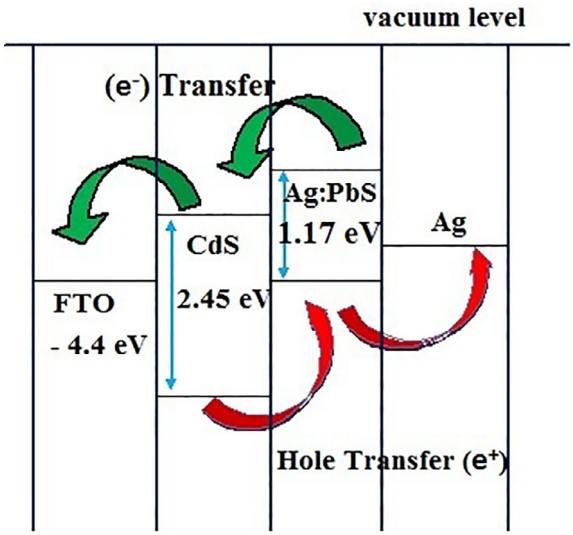

FIGURE 11 Energy band diagram of the prepared FTO/n-CdS/p-PbS:Ag heterojunction [Colour figure can be viewed at wileyonlinelibrary.com]

is decreased on increasing Ag doping concentration up to 6%, so the separation of valance bands has been enlarged. This promotes the production and transfer of carriers and thus increases the photocurrent.

4 | CONCLUSION

In the present study, low-cost nebulizer spray method was used to optimize the Ag level on PbS films for the fabrication of heterostructure devices. From the present work, the major conclusions are as follows:

- The enhancement in crystallite size from 44 to 53 nm was observed for the increase of Ag doping concentration up to 6%, due to the substitution of Ag^{+} into Pb^{2+} ions.
- All the prepared PbS:Ag films have low transmittance, which conforms as absorber material in solar cell, and the obtained band gap is around 1.51 eV.
- Minimum electrical resistivity of about 80 Ωcm was obtained for 6% of Ag-doped PbS film, and it was used to fabricate heterostructure solar cell (n-CdS/p-PbS:Ag) on FTO substrate.
- From the constructed heterostructure, the conversion efficiency was found to be 0.89% for 6% Ag-doped film.

ACKNOWLEDGEMENTS

The authors extend their appreciation to the Research Center for Advanced Materials (RCAMS) at King Khalid University for supporting this work through research project program under grant number RCAMS/KKU/006-19. Thanks to DST for the financial support to purchase research equipment for Arul Anandar College, Tamilnadu, India, through project program under grant number DST-FIST/C-297/2015.

ORCID

S. Rex Rosario https://orcid.org/0000-0002-4337-0023

REFERENCES

1. Green MA, Emery K, Hishikawa Y, Warta W, Dunlop ED. Solar cell efficiency tables (version 46). *Prog Photovolt: Res Appl*. 2015;23:805-812.
2. Tao CS, Jiang J, Tao M. Natural resource limitations to terawatt-scale solar cells. *Sol Energ MatSolC*. 2011;95:3176-3180.
3. Hernández-Borja J, Vorobiev N YV, Ramırez-Bon R. Thin film solar cells of CdS/PbS chemically deposited by an ammonia-free process. *Solar Energy Materials & Solar Cells*. 2011;95:1882-1888.
4. Seghaier S, Kamoun N, Brini R, Amara AB. Structural and optical properties of PbS thin films deposited by chemical bath deposition. *Mater Chem Phys*. 2006;97:71-80.
5. Joshi RK, Sehgal HK. Density of states near Fermi level in PbS nanoparticle films. *Phys E: Low-Dimens Syst Nanostructures*. 2004;23:168-170.
6. Mohamed HA. Theoretical study of the efficiency of CdS/PbS thin film solar cells. *Sol Energy*. 2014;108:360-369.
7. Bhandari KP, Roland PJ, Mahabaduge H, et al. Thin film solar cells based on the heterojunction of colloidal PbS quantum dots with CdS. *Sol Energy Mater sol Cells*. 2013;117:476-482.
8. Beddek L, Messaoudi M, Attaf N, Aida MS, Bougdira J. Sulfide precursor concentration and lead source effect on PbS thin films properties. *J Alloy Compd*. 2016;666:327-333.
9. Fu T. Research on gas-sensing properties of lead sulfide-based sensor for detection of NO_2 and NH_3 at room temperature. *Sens Actuat B*. 2009;140:116-121.
10. Colvin VL, Schlamp MC, Alivisatos AP. Light-emitting diodes made from cadmium selenide nanocrystals and a semiconducting polymer. *Nature*. 1994;370:354-357.
11. Warner JH, Heckenberg N, Rubinsztein-Dunlop H. Non-linear photoluminescence from purified aqueous PbS nanocrystals. *Mater Lett*. 2006;60:3332-3334.
12. Pop I, Nascu C, Ionescu V, Indrea E, Bratu I. Structural and optical properties of PbS thin films obtained by chemical deposition. *Thin Solid Films*. 1997;307:240-244.
13. Gupta BK, Thangaraj R, Agnihotri OP. High absorptivity AlPbS selective surfaces for solar photothermal conversion. *Sol Energy Mater*. 1979;1(5):481-487.
14. Hirata H, Higashiyama K. Analytical study of the lead ion-selective ceramic membrane electrode. *Bull Chem Soc Jpn*. 1971;44:2420-2423.
15. Shen X, Li Z, Cui Y, Pang Y. Glutathione-assisted synthesis of hierarchical PbS via hydrothermal degradation and its application in the pesticidal biosensing. *Int J Electrochem Sci*. 2011;6(8):3525-3535.
16. Pawar SB, Shaikh JS, Devan RS, et al. Facile and low cost chemosynthesis of nanostructured PbS with tunable optical properties. *Appl Surf Sci*. 2011;258:1869-1875.
17. Saikia D, Phukan P. Fabrication and evaluation of CdS/PbS thin film solar cell by chemical bath deposition technique. *Thin Solid Films*. 2014;562:239-243.
18. Moreno-Garcia H, Nair MTS, Nair PK. All-chemically deposited Bi2S3/PbS solar cells. *Thin Solid Films*. 2011;519:7364-7368.
19. Sattarian H, Tohidi T, Rahmatallahpur SH. Effect of TEA on characteristics of CdS/PbS thin film solar cells prepared by CBD. *Mater Sci-pol*. 2016;36:540-547.
20. Das R, Kumar R. Preparation of nanocrystalline PbS thin films and effect of Sn doping and annealing on their structural and optical properties. *Mater Res Bull*. 2012;47:239-246.
21. Rex Rosario S, Kulandaisamy I, Kumar KDA, et al. Deposition of p-type Al doped PbS thin films for heterostructure solar cell device using feasible nebulizer spray pyrolysis technique. *Physica B: Condensed Matter*. 2019;575:411704.
22. Rajesh Kumar R, Das MG, Ganesan V. Preparation of nanocrystalline Sb doped PbS thin films and their structural, optical, and electrical characterization. *Superlattices and Microstructures*. 2014;75:601-612.
23. Rex Rosario S, Kulandaisamy I, Arulanantham AMS, et al. Fabrication and characterization of lead sulfide (PbS) thin film based heterostructure (FTO/CdS/PbS/Ag) solar cell by nebulizer spray method. *Materials Research Express*. 2019;6:056416.
24. Yucel E, Yucel Y. Fabrication and characterization of Sr-doped PbS thin films grown by CBD. *Ceram Int*. 2017;43:413-707.

25. Thangavel S, Ganesan S, Saravanan K. Annealing effect on cadmium in situ doping of chemical bath deposited PbS thin films. *Thin Solid Films*. 2012;520:5206-5210.
26. Puiso J, Tamulevicius S, Laukaitis G, Lindross S, Leskeia M, Snitka V. Growth of PbS thin films on silicon substrate by SILAR technique. *Thin Solid Films*. 2002;403–404:457-461.
27. Gadave. KM, Jodgudri. SA, Lokhande CD. Chemical deposition of PbS from an acidic bath. *Thin Solid Films*. 1994;245(1-2):7–9.
28. Touati B, Gassoumi A, Turki NK. Structural, optical and electrical properties of Ag doped PbS thin films: Role of Ag concentration. *J Mater Sci Mater Electron*. 2007;28(24):18387-18395.
29. Ravisankar S, Balu AR, Nagarethinam VS. Effect of Gd3+ ions on the thermal behavior, optical, electrical and magnetic properties of PbS thin films. *Journal of Electronic Material*. 2018;47:1271-1278.
30. Misra KP, Shukla RK, Srivastava A, Srivastava A. Blueshift in optical band gap in nanocrystalline $Zn_{1-x}Ca_xO$ films deposited by sol-gel method. *Appl Phys Lett*. 2009;95:031901.
31. Pan LL, Li GY, Lian JS. Structural, optical and electrical properties of cerium and gadolinium doped CdO thin films. *Appl Surf Sci*. 2013;274:365-370.
32. Karthick P, DivyaVijayanarayanan S, Suja M, Sridharan K, Jeyadheepan. Opto-electronic properties of fluorine doped tin oxide films deposited by nebulized spray pyrolysis method. *Asian J Applied Sci*. 2015;8:259-268.
33. Kasar RR, Despande NG, Gudage YG, Vyas JC, Sharma R. Studies and correlation among the structural, optical and electrical parameters of spray-deposited tin oxide (SnO_2) thin films with different substrate temperatures. *Physica B*. 2008;403:3724-3729.
34. Rex Rosario S, Kulandaisamy I, Arulanantham AMS, Deva Arunkumar K, Valanarasu S, Hamdy MS. Analysis of Cu doping concentration on PbS thin films for the fabrication of solar cell using feasible nebulizer spray pyrolysis. *Materials Research Express*. 2019;6:056201.
35. Rajashree C, Balu AR, Nagarethinam VS. Substrate temperature effect on the physical properties of spray deposited lead sulfide thin films suitable for solar control coatings. *Int J Chem Tech Res*. 2014;6:347-360.
36. Chattarki AN, Kamble SS, Deshmukh LP. Role of pH in aqueous alkaline chemical bath deposition of lead sulfide thin films. *Mater Lett*. 2012;67:39-41.
37. Sarica E, Bilgin V. Study of some physical properties of ultrasonically spray deposited silver doped lead sulphide thin films. *Mater Sci Semicond Process*. 2017;68:288-294.
38. Gassoumi A, Alleg S, Kamoun-Turki N. Influencing the structural, microstructural and optical properties of PbS nanocrystalline thin films by Mg2+ doping. *J Mol Struct*. 2016;1116:67-71.
39. Muiva C, Sathiaraj T, Maabong K. Effect of doping concentration on the properties of aluminium doped zinc oxide thin films prepared by spray pyrolysis for transparent electrode applications. *Ceram Int*. 2011;37:555-560.
40. Joseph Edison D, Nirmala W, Deva K, et al. Structural, optical and nonlinear optical studies of AZO thin film prepared by SILAR method for electro-optic applications. *Physica B: Condensed Matter*. 2017;523:31-38.
41. Bharathi RN, Sankar S. Mg doping effects on the physical properties of lead sulphide thin films. *Int J ChemTech Res*. 2015;7(2):980-986.
42. Anitha M, Anitha N, Saravanakumar K, Kulandaisamy I, Amalraj L. Effect of Zn doping on structural, morphological, optical and electrical properties of nebulized spray-deposited CdO thin films. *Applied Physics A*. 2018;124:561.
43. Preetha KC, Remadevi TL. Effect of Al incorporation on the structural, morphological, optoelectronic and transport properties of PbS thin films. *Physica B*. 2012;407:4173-4181.
44. Rajashree C, Balu AR, Nagarethinam VS. Influence of Al doping on the structural, morphological and opto-electrical properties of spray deposited lead sulfide thin films. *J Mater Sci Mater Electron*. 2016;27(8):7876-7882.
45. Cao H, Wang G, Zhang S, Zhang X. Growth and photoluminescence properties of PbS nanocubes. *Nanotechnology*. 2006;17:3280-3287.
46. Tohidi T, Jamshidi-Ghaleh K. Optical and structural properties of nanocrystalline PbS thin film grown by CBD on Si(1 0 0) substrate. *Philosophical Magazine*. 2014;94(29):3368-3381.
47. Zhang N, Zou X, Gao Y. Design of solar optical fiber lighting system for enhanced lighting in highway tunnel threshold zone:A case study of Huashuyan Tunnel in China. *International Journal of Photoenergy*. 2015;2015:1-10.
48. Obaid AS, Mahdi MA, Hassan Z, Bououdina M. Preparation of chemically deposited thin films of CdS/PbS solar cell. *Superlattices and Microstructures*. 2012;52(4):816-823.
49. Arulanantham AMS, Valanarasu S, Jeyadheepan K, Kathalingam A. Effect of thermal annealing on nebulizer spray deposited tin sulfide thin films and their application in a transparent oxide/CdS/SnS heterostructure. *Thin Solid Films*. 2018;666:85-93.

How to cite this article: Rosario SR, Kulandaisamy I, Kumar KDA, Ramesh K, Ibrahium HA, Awwad NS. Ag-doped PbS thin films by nebulizer spray pyrolysis for solar cells. *Int J Energy Res*. 2020;1–11. https://doi.org/10.1002/er.5227